IR VULNERABILITY OF MODERN WARSHIPS USING SHIPIR/NTCS

D.A. Vaitekunas[a], J.T. Thompson[a] and F. Reid[b]

[a]W.R. Davis Engineering Limited, 1260 Old Innes Road,
Ottawa, Ontario, Canada, K1B 3V3
ntcs@davis-eng.on.ca

[b]Defence Research Establishment Valcartier, 2459 Pie XI Blvd.,
Val Bélair, Québec, Canada, G3J 1X5
francoise.reid@drev.dnd.ca

ABSTRACT

A number of ongoing ship programs (Norwegian Frigate, US DD-21, Spanish F100) have specified infrared (IR) signatures as part of their overall requirement. These same ship programs are using the NATO-standard IR signature model (ShipIR/NTCS) to predict and evaluate the signatures of their new ship designs. This paper describes the naval threat component of the model (NTCS) and its ability to predict IR vulnerability in terms of an IR detection range. A technical description of the generic NTCS imaging seeker model is provided. The results from a typical mid-wave and long-wave imager, operating under different environmental conditions, against a ship with different levels of IR signature suppression (IRSS), illustrate the benefits of IR signature reduction. Future plans to expand ShipIR/NTCS for the design of flare countermeasures, flare deployment tactics, and active IR signature reduction techniques are also discussed.

1.0 INTRODUCTION

1.1 MODERN WARSHIP DESIGN

The general features and requirements of a modern warship are well described by Calvano and Riedel[(1)] for the Regional Deterrence Ship (RDS 2010):

- operate in any part of the world as both a peacekeeping and tension reducing tool,
- ability to damage the war fighting capability of an aggressor
- project power ashore while minimizing own vulnerability and susceptibility
- pre-attack threat recognition nearly impossible, very short defence reaction times, and high probability of hit

The modern warship requirement emphasizes a need for good self-defence, but also highlights the need for adequate stealth protection. Goddard et al.[(2)] provide a review of arguments justifying the use and cost effectiveness of stealth technology:

- improved operational effectiveness
- enhanced ship survivability
- a vital attribute for littoral warfare
- improved effectiveness of weapons systems
- more ordnance devoted to offensive missions
- improved decoy and EW performance

Although their paper deals entirely with radar cross section (RCS), the same principles can be applied to infrared signature. They emphasize the need for a balanced approach: “One of the keys is to determine the proper balance of

stealth, EW and hard kill systems for our next generation surface combatant."[2]

Most of today's modern warships include some form of infrared signature suppression[3], and the trend is towards a more systematic and comprehensive evaluation of IR signature[4], where the tradeoff between IR signature suppression and associated reductions in IR susceptibility are evaluated. It has long been established that a ship's overall survivability is ultimately a function of its detectibility. Therefore, it is important to provide the ship designer with a tool for evaluating both IR signature and IR detectibility. This way, "soft" prototypes can be evaluated in the early stages of a ship program, before deciding on a particular design. As a result, more effort is being made to provide the simulation and modelling tools for such evaluations.

1.2 SHIPIR/NTCS AS A DESIGN TOOL

ShipIR/NTCS[5,6] is an integrated naval ship, threat and countermeasure model, capable of predicting the infrared signature of naval warships in their maritime background, as shown in Figure 1. Developed in the early 90's for the Canadian Department of National Defence, it has now been adopted by the U.S. Naval Research Laboratory (NRL) for use in various Electronic Warfare and Signature programs, and by the NATO TG.06 (Task Group on Maritime Infrared Target and Background Signatures, Measurement and Characterization) as a NATO-standard ship signature model. There are a total of 26 site licenses worldwide, with 10 in the participating nations of NATO TG.06, 9 in various non-NATO government organisations, and 7 in use by various commercial naval warship design offices.

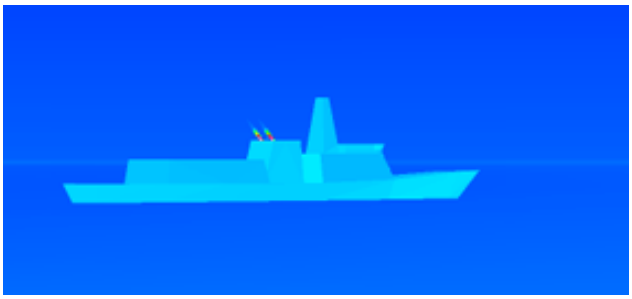

Figure 1: Typical output from SHIPIR.

The ShipIR component of the model, as shown in Figure 2, consists of several sub-models. The background model predicts the thermal and in-band radiance of the sun, sky, atmosphere[7], and sea[8]. A target model based on generalized 3D CAD geometry, a heat transfer model, and complex surface reflectance model are used to predict the in-band target skin signature. A plume model based on empirical stack flow correlations and a spectral gas-band model is used to predict the IR emission of each exhaust plume on the ship. The observer and scenario models are used to view the IR scene interactively (based on observer range, altitude, heading, and selected IR band) and perform both signature and threat engagement analysis. The naval threat and countermeasure simulator component of the model (NTCS) uses the observer and scene models to produce a fly-in engagement between a seeker and any number of navy vessels. The IR image produced by ShipIR is fed into the seeker model for target detection and tracking. Updates in observer position and heading are obtained through proportional navigation on the seeker calculated aim-points, and used to update the IR display at discrete time intervals in the engagement. Flare countermeasures (EW tactics) are defined by specifying the flare emission characteristics and decoy deployment strategies for each target.

Both ShipIR and NTCS are fully-deterministic and physical models, requiring the input of real physical data. Meteorological data, geography, and date/time are used to simulate the maritime background. IR band and spectral response characteristics define the sensor. A bulk of the work to prepare an IR simulation involves the input and specification of a target model. Complex 3D geometry, optical surface properties, trajectory, speed, and onboard power-plant usage are all key elements used to determine the ship signature. To perform an IR analysis of the threat, various relative target aspect information (e.g., relative location, range, speed, heading) and seeker performance data (e.g., NER, FOV, IFOV) are required.

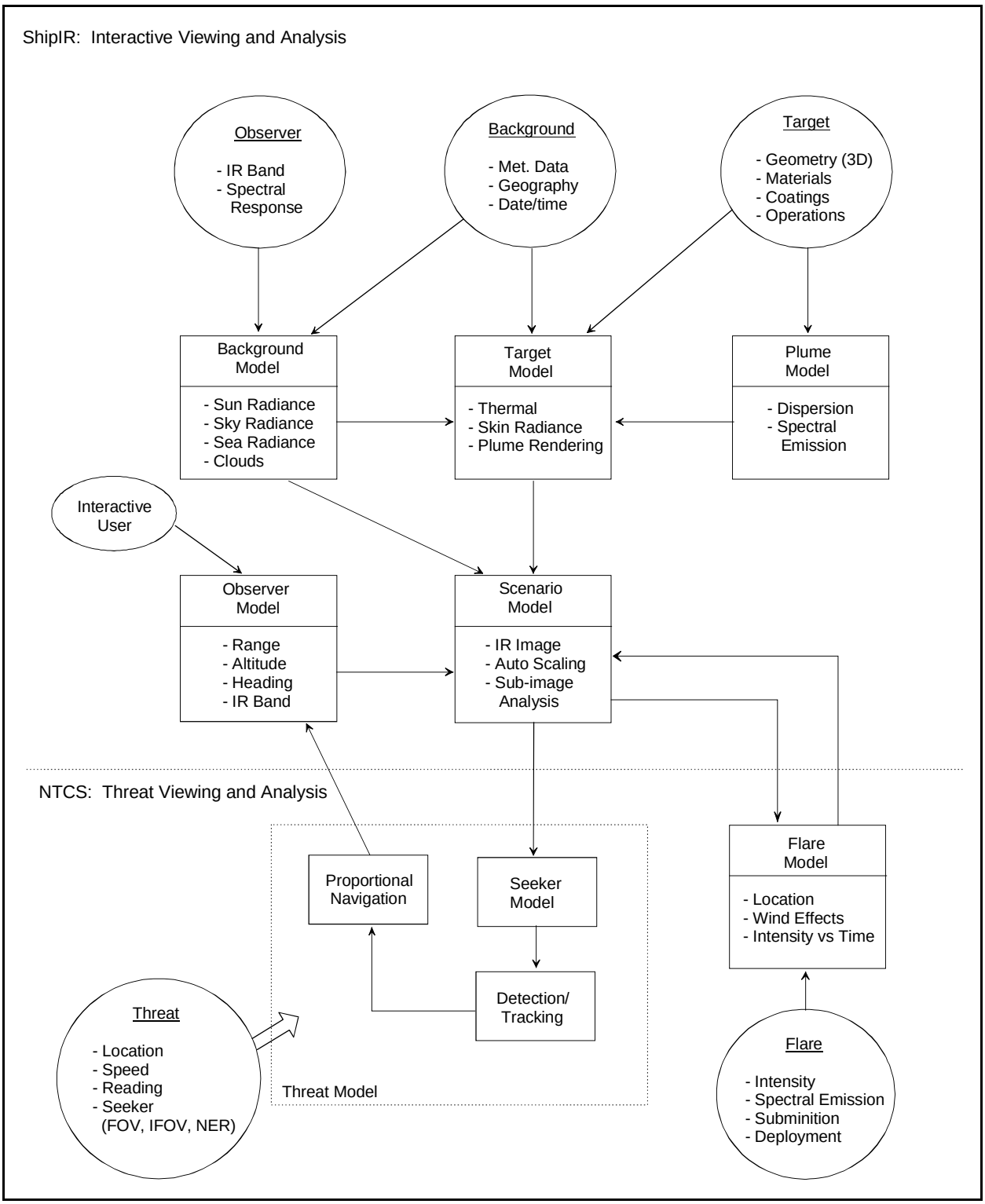

Figure 2: Block diagram of ShipIR/NTCS.

1.3 SAMPLE SIMULATIONS

The generic frigate simulation described in Table 1 is used to illustrate some key features of the ShipIR/NTCS model. Once the simulation has been setup and pre-processed, a number of outputs from the model are used to analyse the IR signature and IR susceptibility of a target. Examples of polar signature and polar detection range plots are shown for the mid-wave (MWIR) and long-wave (LWIR) bands in Figures 3 through 6. In the graphs, DIW refers to

Table 1: Generic frigate IR simulation.

<table>
<tr><th colspan="6">Background Model</th></tr>
<tr><td>Geography</td><td colspan="2">Atmosphere</td><td colspan="3">Observer</td></tr>
<tr><td>longitude: 0°
latitude: 15°
date: 20 June
time: variable</td><td colspan="2">profile: 1976 US Standard
boundary layer: Navy Maritime
visibility: calculated by model
cloud cover: clear sky
wind direction: +270° (South)
current wind speed: 7 m/s
24-hour wind speed: 7 m/s
air temperature: 15°C
sea temperature: 15°C
relative humidity: 80%</td><td colspan="3">altitude: 12 m
spectral response: mtr98
MWIR: 3.36–5.08 μm (Δ=10 cm^{-1})
LWIR: 7.27–13.99 μm (Δ=5 cm^{-1})

<u>Model Options</u>:
sky: MODTRAN
sun: MODTRAN
sea: Cox + Munk
glint: normal
solar scattering: none</td></tr>
<tr><th colspan="6">Target Model(s)</th></tr>
<tr><td>General Arrangement</td><td colspan="2">Stack (no IRSS)</td><td colspan="3">Stack (with IRSS)</td></tr>
<tr><td><u>Geometry</u>:
Length: 133 m
Width: 16 m
Height: 28 m
Waterline: 4.4 m

<u>Propulsion:</u>
2 × G.E. LM2500 gas turbines (GT)
2 × MTU diesel engines (CR)

<u>Speed / Power</u>:
GT = 36 MW = 15 m/s
CR = 12 MW = 10 m/s</td><td colspan="2"><u>GT</u>:
diameter: 1.75 m
flow: 75 kg/s
temperature: 500°C
C0: 0.0020 %-mol.
$C0_2$: 3.20 %-mol.
H_2O: 4.11 %-mol.
soot: 1.68×10^{-9} vol.-frac.

<u>CR</u>:
diameter: 0.8 m
flow: 12 kg/s
temperature: 460°C
C0: 0.0029 %-mol.
$C0_2$: 6.29 %-mol.
H2O: 6.82 %-mol.
soot: 3.73×10^{-9} vol.-frac.</td><td colspan="3"><u>GTS</u>:
diameter: 2.6 m
flow: 176 kg/s
temperature: 220°C
C0: 0.0009 %-mol.
$C0_2$: 1.40 %-mol.
H_2O: 2.54 %-mol.
soot: 1.12×10^{-9} vol.-frac.

<u>CRS</u>:
diameter: 1.0 m
flow: 20 kg/s
temperature: 280°C
C0: 0.0018 %-mol.
$C0_2$: 3.94 %-mol.
H2O: 4.76 %-mol.
soot: 2.94×10^{-9} vol.-frac.</td></tr>
<tr><th colspan="6">Seeker Model(s)</th></tr>
<tr><td>Type</td><td>NETD</td><td>NER</td><td>IFOV</td><td>FOV_x</td><td>FOV_y</td></tr>
<tr><td>MWIR</td><td>0.125 °C</td><td>0.00718 $W/m^2{\cdot}sr$</td><td>1 mrad</td><td>9°</td><td>7.5°</td></tr>
<tr><td>LWIR</td><td>0.125 °C</td><td>0.0612 $W/m^2{\cdot}sr$</td><td>1 mrad</td><td>9°</td><td>7.5°</td></tr>
</table>

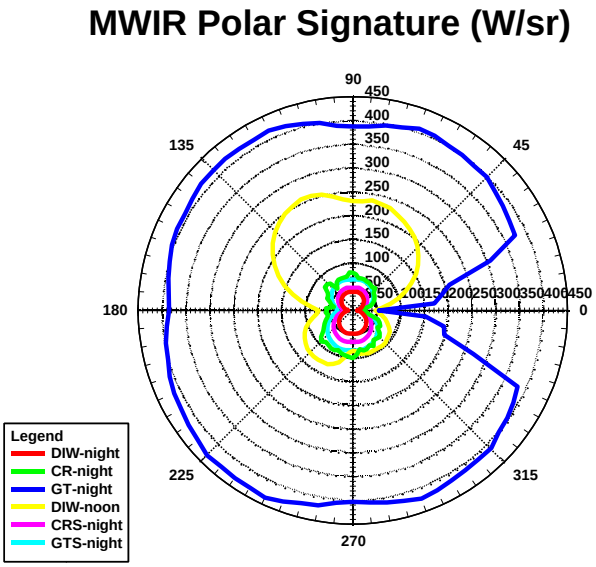

Figure 3: MWIR signature polar plot.

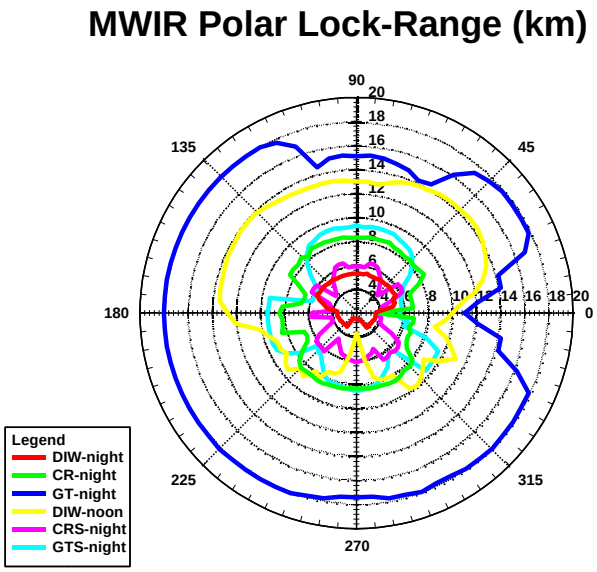

Figure 4: MWIR lock range polar plot.

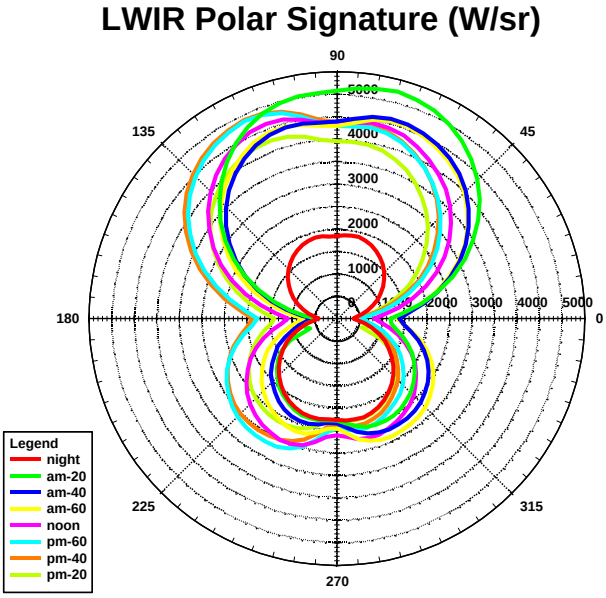

Figure 5: LWIR polar signature plot.

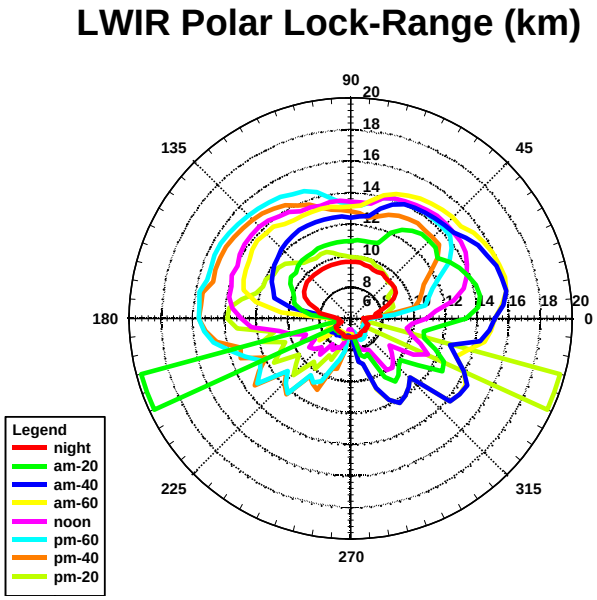

Figure 6: LWIR lock range polar plot.

no ship propulsion (dead-in-water), am-xx / pm-xx refer to morning / afternoon conditions with the sun at a specified elevation angle (xx) in degrees, and (GT, CR, GTS, CRS) refers to gas-turbine and cruise-diesel propulsion, with and without IR suppression (IRSS).

The MWIR results show the following: (1) at certain azimuths, the GT-night and DIW-noon have similar signature and IR detection range, except the full-GT signature emits from all view angles, (2) the CRS-night and DIW-night have a similar signature and IR detection range, indicating an optimal design of the suppressor, and (3) the GTS-night signature and IR detection are similar to the unsuppressed cruise diesel (CR-night), indicating a lower gas

turbine plume temperature would be required to achieve the signature objective of the CRS-night case. The lobes occurring in the polar signature plot are due to variations in projected-area, hull temperature distribution, and surface masking effects (e.g., plume). The IR detection range is much more sensitive to these variations, especially for low-contrasts targets at close-range (e.g., DIW-night, CRS-night), and high-contrast targets at long-range (e.g., GT-night).

The LWIR signature and detection range are typically dominated by skin signature sources, since there is no appreciable plume signature in this wave-band. The daytime runs versus solar angle with no propulsion (DIW) show the peak detection range (14–16 km) to be relatively insensitive to time of day. The aspect-angle variations that do occur in signature and detection range are due to changes in solar azimuth, projected-area, and temperature distribution (e.g., hull, deck, and upper structure). The strong lobes on the cool-side of the ship (shaded from the sun) in the am-20, pm-20, and the am-40 plots are the result of large negative contrasts between the ship and sea background when viewing along the solar azimuth (i.e., solar glint reflections off the sea). It will be shown later that the generic NTCS seeker selects between positive and negative contrast when analysing each contrast image, a feature easily exploited by imaging seekers.

In the past, some have argued against IR suppression of the exhaust plumes, since they have the same signature and detection range as the hull and super structure during the daytime (DIW-noon). However, this neglects the fact that over 50% of the ship's operating cycle is at night (in the absence of sun), and that excessive hull signatures can be reduced or eliminated by the use of appropriate surface IRSS technology[4]. Although not shown, any visible component of the unsuppressed hot metal of the exhaust stack will be detected by an IR missile as soon as it is visible over the horizon. The above examples have assumed an ideal scenario where vertical uptakes (cut flush with the funnel top) show no exposure to a sea-skimming (horizontal) seeker. Some have also argued that such designs require no metal suppression when only considering sea skimming threats. However, this provides zero angle protection from threats originating above the horizon, and allows for no tolerance in ship roll-angle, typically encountered in rough seas and while navigating a turn.

The background and target signature profiles associated with some of the previous signature results are shown in Figures 7 through 10. The apparent temperature of the sea and sky in both bands, shown in Figure 7 versus angle from the horizon, has the following characteristics: (1) the horizon is close to a black body at the air temperature (15°C), (2) a linear decrease in sky radiance looking above the horizon from the decreased thickness and water content of the air, and (3) a sharp decrease in sea radiance just below the horizon from the high ocean reflectance of above-horizon cool sky. These profiles are typical in shape but their magnitude varies considerably with air / sea temperature, relative humidity, cloud cover, and maritime aerosol content of the air. Because of the characteristic vertical profile of the sea / sky background, modern imaging seekers will use horizontal contrasting to maximize their detection of maritime targets. Figure 8 shows the MWIR target contrasts obtained from DIW-night, CR-night, GT-night, and DIW-noon at 500 m off the port-side. The area under these curves is equal to the total contrast intensity used to plot the data at +90° in Figure 3. The apparent contrast temperatures obtained from two of the above examples, shown in Figures 9 and 10, are used to further analyse the spatial distribution of target signature. Apparent contrast temperature is a useful metric to compare images, since both absolute radiance and contrast radiance ($W/m^2 \cdot sr$) vary with background and spectral response of the sensor. These two examples show how the DIW-noon signature is mainly due to the RCS-tilted panels of the upper ship structure, while the GT-night signature is highly concentrated in both area and magnitude around the gas turbine outlet (i.e., plume). Only a small portion of both signatures originate from hull contrasts below the horizon. The GT-night signature also shows a negative contrast between the upper mast structure and the warm sky near the horizon, as these surfaces radiate to a cooler sky above the horizon. This effect is further increased by the 7% tilt-angle typically used to reduce RCS signature.

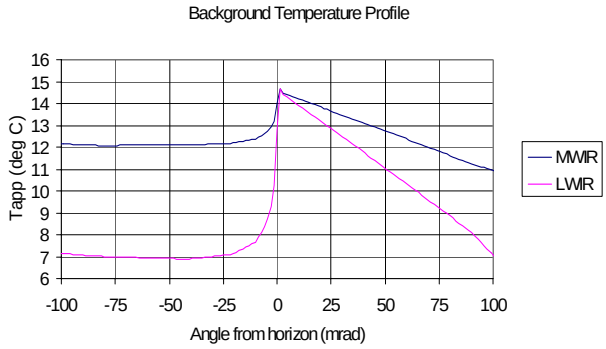

Figure 7: Background signature profile.

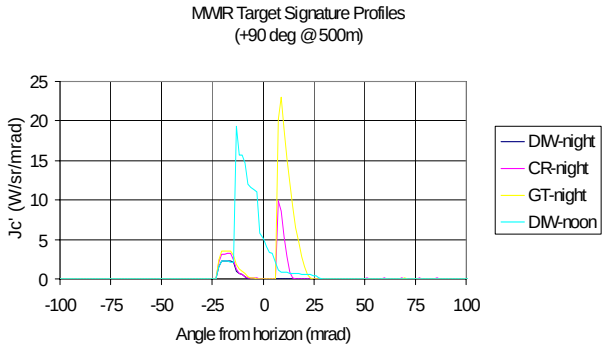

Figure 8: Target contrast signature profile.

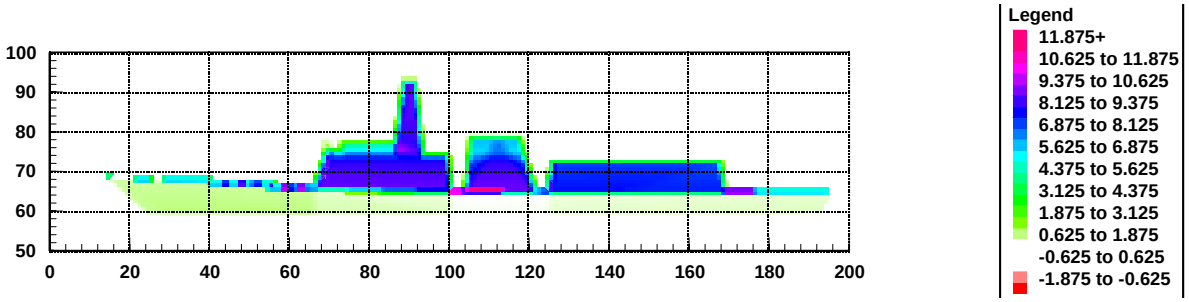

Figure 9: MWIR contrast temperature map (DIW-noon, +90° @ 500 m).

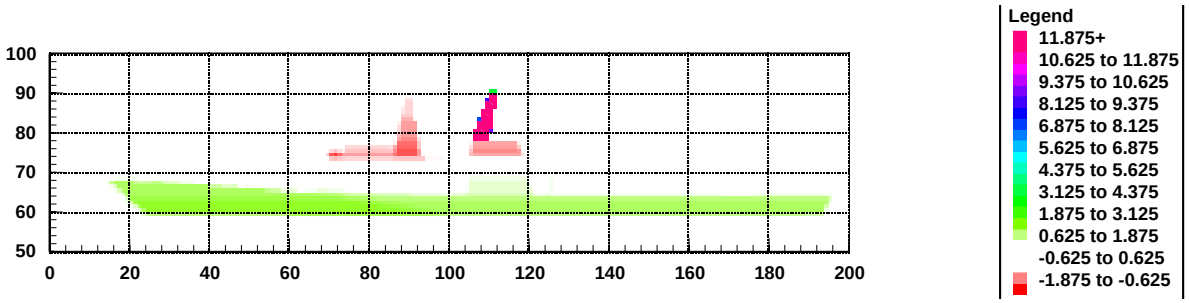

Figure 10: MWIR contrast temperature map (GT-night, +90° @ 500 m).

2.0 IR DETECTION

According to the IR/EO Handbook[9], there are three basic types of detection pertinent to target acquisition modelling:

- Detection: a temporally unconstrained perception of an object at a specific display field location.
- Pure detection: detection where the two alternative choices are (1) that something is present or (2) that nothing is present.
- Discrimination detection: a detection where the two alternative choices are (1) the object is a target or (2) the object is something else, such as a natural scene element.

Traditionally, the target acquisition process is broken up into two distinct parts:

- Search tasks: the position of the target is unknown, and the time to locate the target is of fundamental importance.
- Static tasks: the observer has as much time as desired to perform the operation of detection, recognition, or identification.

The process of IR detection used by NTCS is a static performance measure based on pure detection, where the target is assumed within the display field and the detection criteria alone dictates whether something is present (i.e., no specialized target search required).

2.1 SENSOR CHARACTERISTICS

The following EO sensor characteristics are used to define the static performance of an IR imaging sensor:

- Noise-equivalent temperature difference (NETD): the temperature difference between a "large" target (i.e., at least 10× the subtense of the detector) and its background (i.e., uniform background temperature) required to produce a peak signal equal to one rms noise level.

- Noise-equivalent radiance (NER): equivalent to NETD, except the signal is expressed in units of radiance ($W/m^2 \cdot sr$) instead of temperature (°C). Since EO systems typically operate in a range where the response between the detector voltaic output and the apparent radiance is linear, one can assume a constant NER for the system at a particular value of gain and DC offset[10].

- Spectral response filter (SRF): the normalized spectral response of the detector and optical system, as shown in Figures 11 and 12, used to calculate the functional relation between apparent radiance (L_{app}) and apparent temperature (T_{app}), as shown in Figure 13:

$$L_{app} = \int_0^\infty \tau_{opt}(\lambda) L_{bb}(T_{app}, \lambda)\, d\lambda \tag{1}$$

L_{bb} is the radiance of a perfect black body. The NER can be calculated from the NETD (ΔT_{ref}) and associated background temperature (T_{ref}) as follows:

$$NER = \int_0^\infty \tau_{opt}(\lambda)\left[L_{bb}(T_{ref} + \Delta T_{ref}, \lambda) - L_{bb}(T_{ref}, \lambda) \right] d\lambda \tag{2}$$

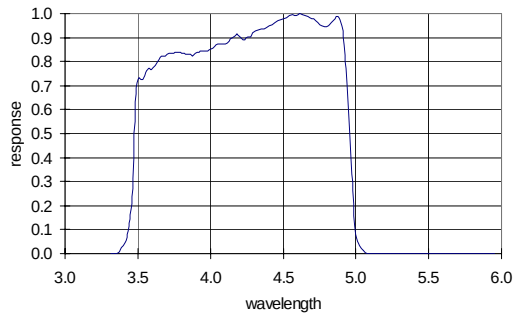

Figure 11: Sample spectral response (MWIR).

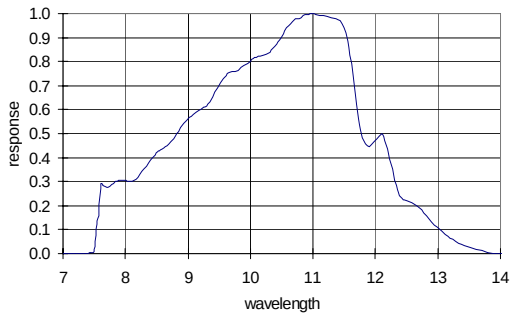

Figure 12: Sample spectral response (LWIR).

- Instantaneous field-of-view (IFOV): the angular subtense of a single-detector or single-pixel in the output device.

- Resolution (m×n): the total number of detectors or pixels in the horizontal (m) and vertical (n)

direction.

2.2 ANALYTICAL DETECTION

Based on the previous EO sensor relations and characteristics, one can use the following six step procedure to calculate the probability of pure detection for a target at a specified range (R). To simplify the calculations, a uniform black body temperature is assumed for both the background (T_{bck}) and target (T_{tgt}), and the total area projected by the target towards the sensor is defined as A_T.

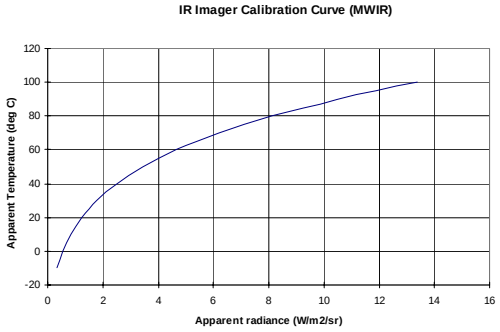

Figure 13: Radiance versus temperature (MWIR).

Step 1: Calculate the apparent background radiance:

$$L_{bck} = \int_0^\infty \tau_{opt}(\lambda)\left[\tau_{atm}(R,\lambda)\,L_{bb}(T_{bck},\lambda) + L_{atm}(R,\lambda)\right]d\lambda \tag{3}$$

For a uniform temperature background with no solar path-scattering:

$$L_{atm}(R,\lambda) = \left[1 - \tau_{atm}(R,\lambda)\right]L_{bb}(T_{bck},\lambda) \tag{4}$$

$$\therefore\ L_{bck} = \int_0^\infty \tau_{opt}(\lambda)\,L_{bb}(T_{bck},\lambda)\,d\lambda \tag{5}$$

Step 2: Calculate the apparent target radiance:

$$L_{tgt} = \int_0^\infty \tau_{opt}(\lambda)\left[\tau_{atm}(R,\lambda)\,L_{bb}(T_{tgt},\lambda) + L_{atm}(R,\lambda)\right]d\lambda \tag{6}$$

Step 3: Calculate the apparent target-pixel radiance within a single IFOV of the sensor:

$$\bar{L}_{tgt} = \left(\frac{A_T}{A_c}\right)L_{tgt} + \left(1 - \frac{A_T}{A_c}\right)L_{bck} \tag{7}$$

where:

$$A_c = \begin{cases} A_T\ , A_T > A_o \\ A_o\ , A_T \le A_o \end{cases} \qquad A_o = \left(R\cdot IFOV\right)^2 \tag{8}$$

Step 4: Calculate the apparent target-pixel contrast radiance:

$$\Delta L_{tgt} = \bar{L}_{tgt} - L_{bck} \tag{9}$$

Note that when the target (A_T) occupies less than four IFOV's of the sensor ($4\times A_o$), the above-calculated target-pixel contrast is the maximum possible for detection since this value can be equally divided by as many as 4 adjacent pixels in the sensor FOV.

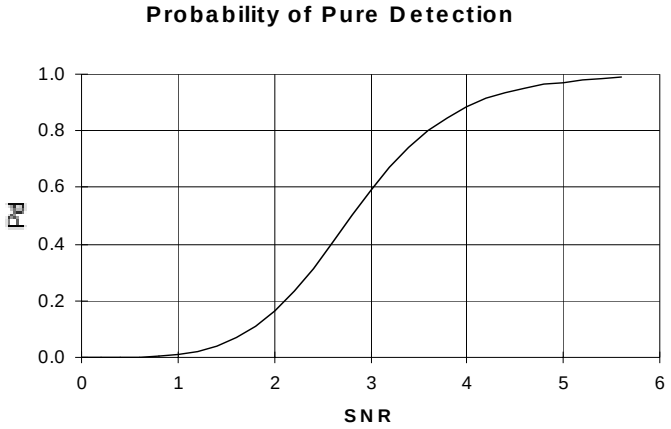

Figure 14: Probability of pure detection (P_d).

Step 5: Calculate the signal-to-noise ratio of the target-pixel:

$$SNR = \frac{\Delta L_{tgt}}{NER} \tag{10}$$

Step 6: Based on the signal-to-noise ratio and the empirical results from Rosell and Wilson[11], the probability of detection (P_d) is calculated using the following approximate relation (see Figure 14):

$$P_d = \frac{\left(SNR/SNR_{50}\right)^E}{1 + \left(SNR/SNR_{50}\right)^E} \tag{11}$$

$$E = a + b\left(SNR/SNR_{50}\right) \qquad a = 4 \qquad b = 1.2 \qquad SNR_{50} = 2.8 \tag{12}$$

When performing the previous IR detection analysis on the generic frigate, a value of $SNR = 5.0$ was used (i.e., $P_d \approx 1.0$).

2.3 NTCS SEEKER DETECTION

The NTCS seeker detection algorithm functions in a manner similar to the previous analytical detection algorithm, except more sophisticated IR imaging capabilities are used to model the target and background. The basic steps involved are the following:

Step 1: The NTCS image is updated according to the position and orientation of the target(s), flare(s), and missile at the current time step in the engagement. These images incorporate two important analysis features[12]:

- The minimum and maximum radiance are scaled automatically to ensure the image is neither saturated in the "black" or "white" of the colour scale, similar to the automatic gain control (AGC) of an IR sensor, maximizing the available pixel colour resolution.
- A sub-image analysis algorithm detects when the target can be redrawn an integer multiple of its size within the main window (800×600), and sub-sampled back into the main window, maximizing available pixel spatial resolution.

Step 2: A seeker raw image is sub-sampled from the main window and fed into the seeker algorithm. The gain and offset of the imager are assumed to match the zero and maximum radiance of the raw image sampled at every time step (i.e., no temporal filtering). As a result, the maximum radiance sampled by the seeker appears "white"in the first of three seeker analysis windows.

Step 3: The raw seeker image is then contrasted using the following horizontal contrast algorithm to produce the second of three seeker analysis windows:

$L(i,j)$ = radiance value at column (i) and row (j) in the seeker array (m×n)

$\bar{L}(j)$ = average (horizontal) radiance along row (j):

$$\bar{L}(j) = \frac{1}{m} \sum_{i=1}^{m} L(i,j) \tag{13}$$

$L_c(i,j)$ = horizontal contrast radiance at column (i) and row (j):

$$L_c(i,j) = L(i,j) - \bar{L}(j) \tag{14}$$

A bias between positive and negative contrast is used to maximize the detected target signal:

$$\text{bias}(j) = \begin{cases} + & , L_{c,\max}(j) \geq \left| L_{c,\min}(j) \right| \\ - & , L_{c,\max}(j) < \left| L_{c,\min}(j) \right| \end{cases} \tag{15}$$

where

$$L_{c,\max}(j) = \max\left(L_c(i,j),\ i = 1,m\right) \tag{16}$$

$$L_{c,\min}(j) = \min\left(L_c(i,j),\ i = 1,m\right) \tag{17}$$

Such that,

$$L'_c(i,j) = \begin{cases} \max\left(L_c(i,j) - \bar{L}(j), 0\right) & , \text{bias}(j) = + \\ \max\left(\bar{L}(j) - L_c(i,j), 0\right) & , \text{bias}(j) = - \end{cases} \tag{18}$$

Step 4: Depending on which one of three basic imaging types is used, the following seeker relations are applied to the contrast radiance image to produce the last of three seeker analysis windows:

$L_{c,\text{det}}$ = contrast radiance threshold for detection

$$L_{c,\text{det}} = SNR \times NER \tag{19}$$

- Binary centroid:

$$B_c(i,j) = \begin{cases} 1 & , L'_c(i,j) \geq L_{c,\text{det}} \\ 0 & , L'_c(i,j) < L_{c,\text{det}} \end{cases} \tag{20}$$

- Intensity centroid:

$$I_c(i,j) = \begin{cases} L'_c(i,j) & , L'_c(i,j) \geq L_{c,\text{det}} \\ 0 & , L'_c(i,j) < L_{c,\text{det}} \end{cases} \tag{21}$$

- Threshold intensity centroid:

$$I_c(i,j) = \begin{cases} L'_c(i,j) & , L'_c(i,j) \geq L_t \\ 0 & , L'_c(i,j) < L_t \end{cases} \tag{22}$$

where

$$L_t = \max\left(L_{c,\text{det}}, R_t \times L'_{c,\max}\right) \tag{23}$$

$$L'_{c,\max} = \max\left(L'_c(i,j)\ ,\ i=1,m\ ,\ j=1,n\right) \tag{24}$$

R_t is a threshold coefficient (0–1), used to focus the seeker aim-point on the area of highest contrast.

Step 5: A two-criteria detection algorithm: the number of consecutive frames ($N_f \geq N_{f,\text{det}}$) and the number of pixels ($N_p \geq N_{p,\text{det}}$) required for detection, is used to establish the lock-on condition. Once lock-on is established, the above threshold contrast image is used to calculate the seeker centroid or aim-point used by the missile IR guidance algorithm. Values of $N_{p,\text{det}}=1$ and $N_{f,\text{det}}=2$ were used for all the detection range analysis presented in this paper.

To illustrate some of the features in the NTCS seeker algorithm, various seeker contrast profiles and time histories are presented in Figures 15 through 18. Figure 15 shows the contrast profile from the LWIR seeker at 10 km from the port-side of the DIW-noon frigate. All four rows of the seeker with detectible contrast (73–76) show a positive bias with the background. Figure 16 shows the contrast profiles for the same LWIR seeker at 2 km from the port-side of the DIW-night frigate, where a combination of positive (69–72) and negative (73–82) bias occurs in the seeker contrast. Slanting of surfaces on the upper structure of the ship for the purpose of RCS reduction is the source of this negative contrast (i.e., these facets face a cooler part of the sky). The time histories for both the MWIR and LWIR seeker, shown in Figures 17 and 18, respectively, trace the peak signal-to-noise ratio as a function of range from the target. They show how the detailed imaging seeker analysis can be used to perform IR detection analysis. By evaluating the fly-in engagement up to the point of detection (SNR=5) for a number of target azimuths, the polar lock-range plots in Figures 4 and 6 are obtained.

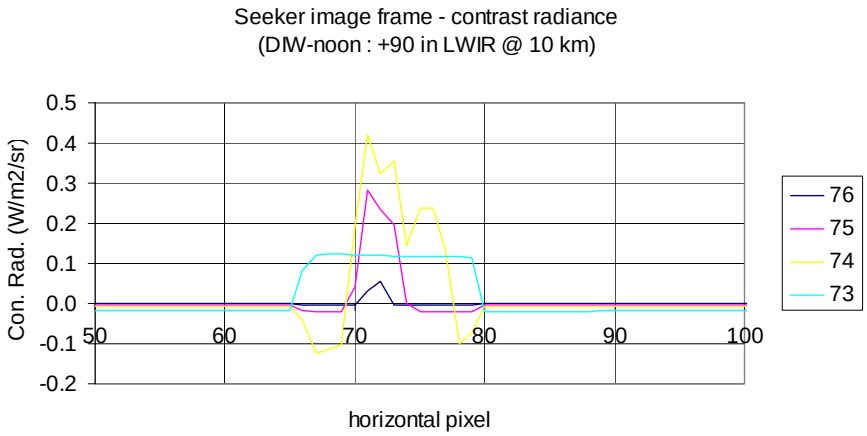

Figure 15: Seeker contrast with positive bias only.

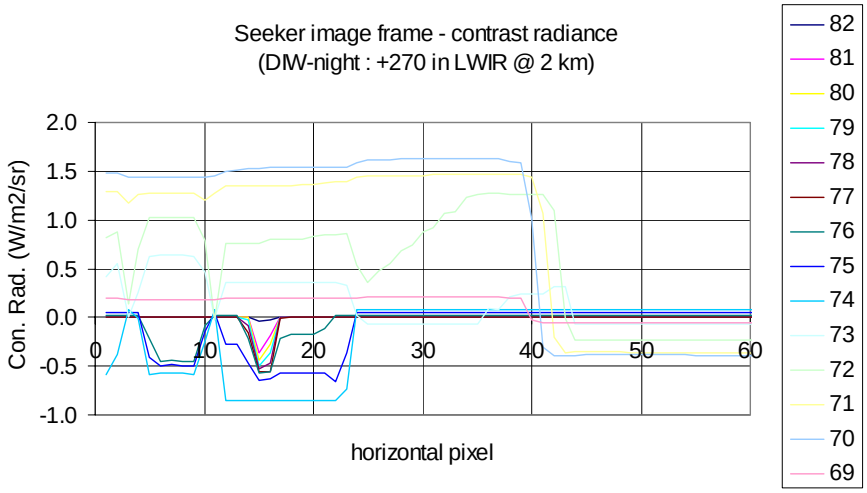

Figure 16: Seeker contrast with positive and negative bias.

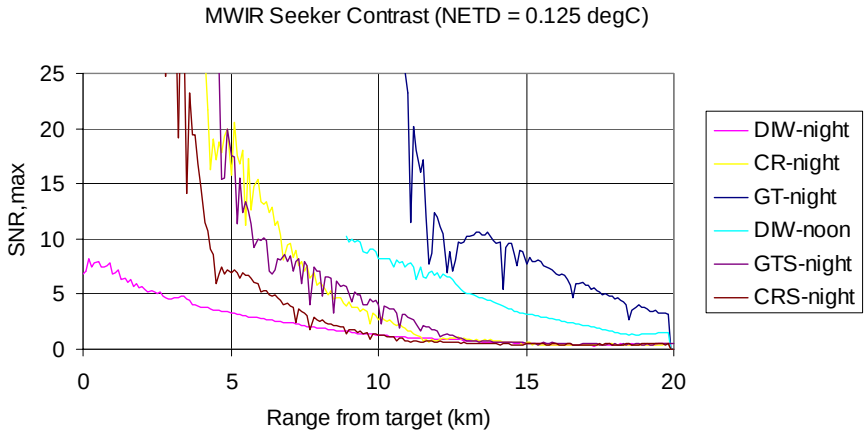

Figure 17: MWIR seeker time histories.

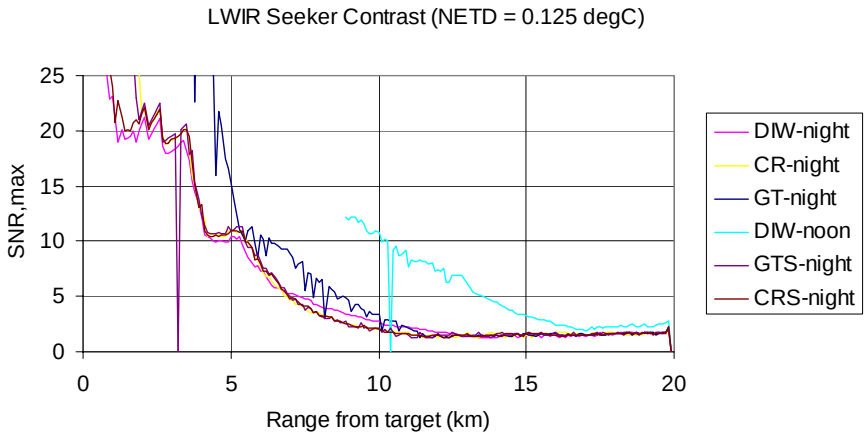

Figure 18: LWIR seeker time histories.

3.0 DEFINITION OF IR SUSCEPTIBILITY

From the peak signal-to-noise ratio (SNR) in the seeker (Figures 17 and 18), the probability of detection can be computed as a function of seeker range using Equation (11), as shown in Figure 19. From these results, we observe the following:

- The probability of detection will never be eliminated entirely.
- The benefits of IR signature reduction are twofold: (1) the IR susceptibility of the target is reduced (i.e., the threat must come in closer to achieve the same probability of detection), and (2) there is more time available to respond with EW decoys and hard kill.

The change in lock range between the different signature configurations is more or less constant, regardless of the SNR

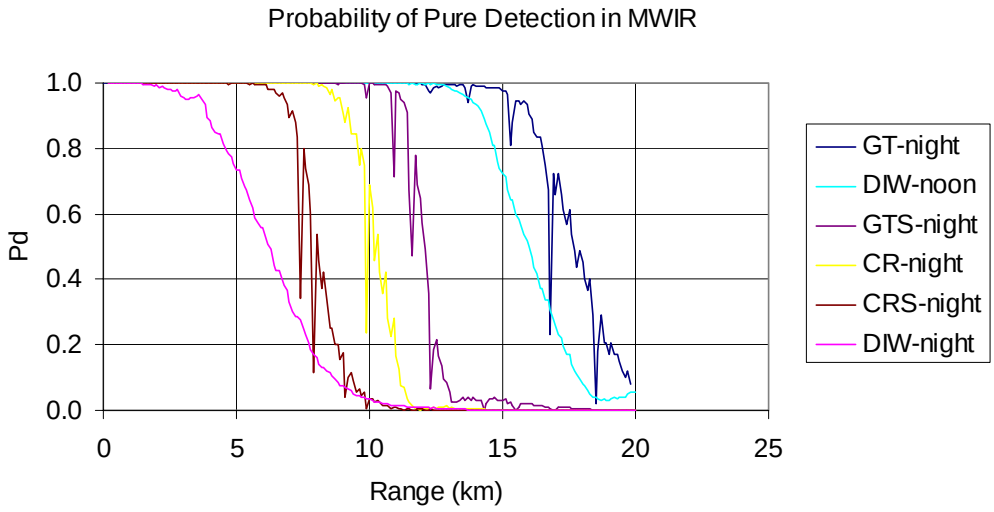

Figure 19: Probability of detection based on seeker time histories.

value used. Therefore, the following simple formulas can be used to estimate the change in IR susceptibility and increased response time for each IR signature reduction:

$$S = \text{IR Susceptibility} = \frac{R_{lock}}{R_{base}} \tag{25}$$

$$\Delta T_{resp} = \text{additional time to respond} = \frac{R_{base} - R_{lock}}{V_c} \tag{26}$$

The results obtained from these two equations for the data shown in Figure 19 are summarized in Table 2, assuming a V_c of 300 m/s. Significant reductions in IR susceptibility (50–60%) are achieved through IR signature reduction. The DIW-night case provides a useful metric to measure future (advanced) IRSS techniques, since it represents the lowest possible IR signature.

Table 2: IR Susceptibility results obtained from MWIR band.

Run	SNR = 5.0		
	IR Detection Range (km)	IR Susceptibility	Additional Time to respond (sec)
GT-night	17.4	1.0	0.0
DIW-noon	13.1	0.75	14
GTS-night	8.9	0.51	28
CR-night	8.4	0.48	30
CRS-night	6.2	0.36	37
DIW-night	2.6	0.15	49

4.0 FUTURE WORK

As ShipIR/NTCS is accredited for use in new ship programs, and the models of existing ships are validated, the attention will turn to the IR simulation of an appropriate tactical response. The following is a synopsis of future enhancements planned for the model.

- Background clutter: detection range analysis in this paper has assumed a single NETD for the entire FOV of the sensor. This should be compared with more extensive IR measurements of the background (see Figure 20) to show how the average and standard deviation in apparent background temperature (Tapp) varies with look down angle. The existing sea model[8] already predicts an rms variance in sea radiance, but more detailed validation is required before any resultant clutter profiles can be added to the NTCS seeker model.

- Tracking gates: a typical counter-countermeasure (CCM) used by the missile to avoid being seduced by flares launched after the initial detection of the ship. This would allow the

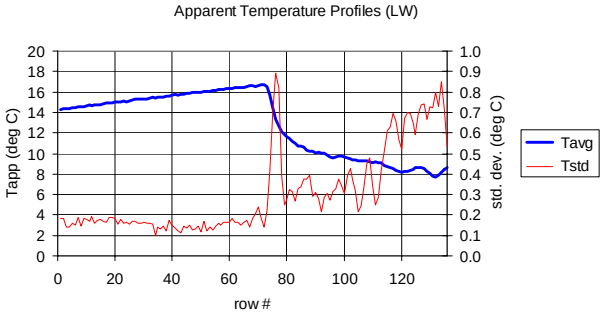

Figure 20: Measured trial background profile (LWIR).

tactical simulation of both distraction and seduction modes of the engagement. In distraction mode, the ship has not yet been detected, so that a flare launched in any direction will probably distract the seeker. In seduction mode, the decoy must be launched within the tracking gate for it to be considered. This feature of the engagement also supports the postponement of IR detection, since more response time is given to launch a distraction flare.

- Flare model: the flare is currently modelled as a black body with a spherical (dynamic) cloud of specified area. The maximum intensity does vary with time, following an exponential rise and fall. To accurately model the flare's emission in all possible IR sensor bands, it is necessary to introduce a spectral emission and rendering algorithm for the flare, similar to the one used by the plume, and allow a variable area profile to be specified as a function of time.

- Transient thermal analysis: the current model only implements a steady-state solution to the highly-coupled generalized heat conduction equation, where both radiation and conduction are solved simultaneously. To improve the analysis capability, it is proposed that thermal properties (i.e., thickness, thermal conductivity, specific heat and density) be added to the model, and that the thermal model be extended to include such diurnal variations as background sun location and active hull cooling. Active hull cooling refers to a special water spray system used to cool down the solar heated surfaces of the ship. The modified form of this model should also include various thermal and in-band reflectance properties of thin liquid films.

5.0 SUMMARY AND CONCLUSIONS

Some of the requirements and objectives of a modern warship have been described, including the effectiveness of IR stealth technology. The integrated naval ship, threat, and countermeasure model (ShipIR/NTCS) was introduced using a series of generic frigate IR simulations to illustrate its suitability for use in IR signature management.

The basic theory of IR detection was used to describe the key sensor characteristics of an IR imaging seeker, provide a simple analytical procedure for predicting the probability of detection of a uniform target in a uniform background, and extend these same procedures to the generic NTCS imaging seeker. The important features of the NTCS seeker model are: (1) a sophisticated IR scene model, (2) horizontal seeker contrasting, and (3) an automatic bias to select between positive and negative contrasts.

The probability of detection obtained from different targets, as a function of range, was used to determine the reductions in IR susceptibility associated with IR signature reduction, and the resultant increases in response time. Future enhancements to the model could include structured background clutter, the incorporation of tracking gates, improvements to the spectral emission and area of the flare model, and the ability to analyse thermal transients. This analysis was performed for a limited set of test conditions, not necessarily representative of all ship operating scenarios, and further plume signature reductions are possible with use of an advanced water injection system[4].

6.0 REFERENCES

1. Calvano, C.N. and Riedel, Lt. J.S. (USN), "The Regional Deterrence Ship (RDS 2010)," *Naval Engineers Journal*, vol. 108, January 1996, pp. 61-72.

2. Goddard, Cdr. C.H. (USN), Kirkpatrick, D.G, Rainey, P.G., and Ball, J.E., "How Much Stealth?," *Naval Engineers Journal*, vol. 108, May 1996, pp. 105-116.

3. Thompson, J., Vaitekunas, D., and Birk, A.M., "IR Signature Suppression of Modern Naval Ships," *ASNE* 21st Century Combatant Technology Symposium, 27-30 January 1998.

4. Thompson, J., Vaitekunas, D., and Brooking, B., "Lowering Warship Signatures: electromagnetic and Infrared,"

SMI Conference on "Signature Management – The Pursuit of Stealth," London, 21-22 February 2000.

5. Morin, J., Reid, F., and Vaitekunas, D., "SHIPIR: a model for simulating infrared images of ships at sea," *SPIE* **2223**, 1994.

6. Vaitekunas, D.A., Alexan, K., Lawrence, O.E., and Reid, F., "SHIPIR/NTCS: a naval ship infrared signature countermeasure and threat engagement simulator," *SPIE* **2744**, pp. 411–424, 1996.

7. Berk, A., Bernstein, L.S., and Robertson, D.C., "MODTRAN: A Moderate Resolution Model for LOWTRAN7," AFGL-TR-89-0122, 1989.

8. Mermelstein, M.D., Shettle, E.P., Takken, E.H., and Priest, R.G., "Infrared radiance and solar glint at the ocean-sky horizon," *Appl. Opt.* **33** (25), pp. 6022–6034, 1994.

9. Howe, James D., "Electro-Optical Imaging System Performance Prediction," Chapter 2, Volume 4, *The Infrared & Electro-Optical Systems Handbook*, ERIM and *SPIE* Press, USA, 1993.

10. Patchan, R.M., "Absolute radiometric techniques and error analysis for imaging radiometers in a field environment," *SPIE* **2470**, pp. 224-235, 1995.

11. Rosell, F.A and Wilson, R.H., "Performance synthesis (electro-optical sensors)," Technical Report AFAL-TR-71-137, AD 884829, Air Force Avionics Laboratory, Wright Patterson Air Force Base, Ohio, USA, May 1971.

12. Vaitekunas, D.A. and Lawrence, O.E., "Infrared scene capabilities of SHIPIR," *SPIE* **3699**, pp. 92–102, 1999.